Controlled Sparse and Percolating Cross-Linking in Waterborne Soft Adhesives

F. Deplace,[†] C. Carelli,[†] A. Langenfeld,[†] M. A. Rabjohns,[‡] A. B. Foster,[‡] P. A. Lovell,[‡] and C. Creton*,[†]

Laboratoire de Physico-Chimie des Polymères et des Milieux Dispersés, UMR 7615, UPMC, CNRS-ESPCI, 10 Rue Vauquelin, 75231 Paris Cédex 05, France, and Materials Science Centre, School of Materials, The University of Manchester, Grosvenor Street, Manchester M1 7HS, United Kingdom

ABSTRACT The effect of low levels of cross-linking on the adhesive and mechanical properties of waterborne pressure-sensitive adhesives was investigated. We have taken advantage of a core–shell latex particle morphology obtained by emulsion polymerization to create a heterogeneous structure of cross-links without major modification of the monomer composition. The latex particles comprise a shell containing cross-linkable diacetone acrylamide (DAAM) repeat units localized on the periphery of a slightly softer core copolymer of very similar composition. Adipic acid dihydrazide was added to the latex prior to film formation to react with DAAM repeat units and affect interfacial cross-linking between particles in the adhesive films. The honeycomb-like structure obtained after drying of the latex results in a good balance between the dissipative properties required for adhesion and the resistance to creep. The characterization of the mechanical properties of the films shows that the chosen cross-linking method creates a percolating lightly cross-linked network, swollen with a nearly un-cross-linked component. With this cross-linking method, the linear viscoelastic properties of the soft films are nearly unaffected by the cross-linking while the nonlinear tensile properties are greatly modified. As a result, the long-term shear resistance of the adhesive film improves very significantly while the peel force remains nearly the same. A simple rheological model is used to interpret qualitatively the changes in the material parameters induced by cross-linking.

KEYWORDS: adhesion • core–shell particles • cross-linking • nonlinear properties

1. INTRODUCTION

In order to be effective, a pressure-sensitive adhesive (PSA) requires a balance of cohesive strength and dissipative properties. Cohesive strength is normally obtained with a light but carefully controlled level of chemical cross-linking of the base polymer. However, because the material also needs to be highly viscoelastic to resist detachment from a surface, the design of a PSA focuses on how to achieve the optimum compromise between these two antagonist properties.

A precise control of the cross-linking is particularly important in the case of PSAs comprising acrylic polymers whether in solution or in dispersion (1, 2). There is, however, a fundamental difference between acrylic PSAs made by solution polymerization and those made by emulsion polymerization. While solution acrylics are usually post-cross-linked and form a continuous network, polymers synthesized by emulsion polymerization are naturally cross-linked inside each particle and form microgels during the synthesis (2−4) as a consequence of the coupling of propagating branches generated through chain transfer to a polymer (5). The final film is then formed by the coalescence of individual particles into a film. In order to obtain a macroscopically strong film, the polymer chains must interdiffuse at the interfaces between the particles (6, 7). This is, of course, not a problem for the polymers of low glass transition temperature (T_g) used for adhesives but results in interfaces that remain weaker than the particles and a lightly cross-linked network that is not continuous, as pointed out by Tobing and Klein (2); this typically leads to a much worse resistance to shear for an equivalent peel force.

A simple way to control the cross-linking in acrylic copolymers is to use a chain-transfer agent (CTA) or a cross-linker during the polymerization. This strategy is widely used in emulsion polymers to control the level of cross-linking in each particle (2, 3, 8, 9). The best compromise between the adhesive strength and resistance to shear is then typically obtained for an intermediate amount of one or more components determined empirically and depending on the monomer composition. However, because the CTA or the cross-linking agent acts on all growing chains, the entire distribution of chain lengths and cross-link density are shifted to higher or lower values. This strategy has reached its limits in terms of optimization, and new thinking is required.

Some hints can be obtained from the recent theoretical developments and experimental observations of the details of the debonding of a PSA. The two criteria that the PSA must satisfy are as follows:

(1) The ratio $\tan \delta(\omega)/G'(\omega)$ must be above $0.5 \times 10^{-5} \, \text{Pa}^{-1}$ to trigger bulk deformation in the adhesive upon debonding, which is necessary for a high peel force.

(2) The Mooney stress in a tensile experiment must have a well-defined minimum at large strain. The higher the value

of the reduced stress at the minimum, then the better the resistance to shear.

The first criterion comes from the balance between resistance to crack propagation and deformability, and the second criterion comes from the necessity to avoid polymer flow. Both criteria have been reviewed and discussed in previous publications (10−12).

In this work, we focus on a specific strategy to design the network structure of the PSA film, taking advantage of the mechanism of film formation from latexes. The strategy consists of activating a cross-linking reaction between latex particles during the drying stage, as opposed to the cross-linking that occurs within the latex particles during latex synthesis. Additionally, it is possible to take advantage of the core−shell particle morphology to create a heterogeneously cross-linked structure. A more cross-linked shell is localized on the periphery of a soft less cross-linked core. With such a structure, it is possible to achieve a different network architecture than that with a pre-cross-linked particle and to create an opportunity to gain a more favorable balance between the adhesion and cohesion of the material. A similar strategy has been previously reported, but the cross-linking monomer was distributed evenly in the particle (8).

We begin with a description of the materials and the cross-linking strategy used, which has been described in more detail elsewhere (13, 14). Then, the effect of the activation of the cross-linking between particles on adhesive and mechanical properties will be shown. In a previous paper (14), we reported extensive studies on similar core−shell latex systems using standard industrial PSA tests to elucidate the important parameters in controlling the adhesive performance. In the present paper, simpler, more model core−shell PSA latexes have been prepared and the focus is on the nonlinear large-strain properties. A viscoelastic-hardening tensile model described elsewhere (13) is used as a tool to interpret the tensile and tack results.

2. MATERIALS AND METHODS

Materials. We performed our experiments with a particular class of materials, model soft core−shell PSAs synthesized using a two-stage monomer-starved semibatch emulsion polymerization process similar to that reported previously (14). The core and shell were formed directly in sequence in a single preparation. The conversion of core monomers was taken to 96−97% conversion before starting polymerization of the shell monomers. The blend of monomers used for the syntheses of both the core and the shell was designed to obtain soft acrylic copolymers. The latexes were made of random copolymers of 2-ethylhexyl acrylate (2-EHA; glass transition temperature of the homopolymer, $T_g = -50$ °C (15)), butyl acrylate (BA; $T_g = -54$ °C (15)), ethyl acrylate (EA; $T_g = -24$ °C (15)), methacrylic acid (MAA; $T_g = 228$ °C (15)), acrylic acid (AA; $T_g = 106$ °C (15)), and styrene (S; $T_g = 100$ °C (15)) as the main monomers.

Diacetone acrylamide (DAAM) was included in the shell comonomer mixture in order to provide functional groups for cross-linking. The DAAM-functionalized particles form cross-links by reaction of the ketone carboxyl with a water-soluble hydrazide during film formation and drying at room temperature, as shown in Figure S1 of the Supporting Information. The density of cross-linking points depends on the concentration of

Table 1. Core and Shell Latex Monomer Compositions of the Core−Shell Particle Studied

	C80dxS20D0.4		
monomer	average	core	shell
2-EHA	66	66	66
EA	15	15	15
BA	10	10	10
S	5	5	5
AA	2	2.5	
sipomer β-CEA	1.2	1.5	
MAA	0.4		2
DAAM	0.4		2
n-dodecylmercaptan (DDM)[b]	0.087	0.1 or 0.15	0.037

[a] "x" has to be replaced by the amount of CTA in the core. [b] CTA, % relative to the total monomer in each phase.

the DAAM groups in the shell and also on the amount of adipic acid dihydrazide (ADH) postadded to the latex prior to film formation.

Two base latexes differing only in the amount of CTA used for the core (0.1 and 0.15 wt % to monomer, respectively) were used in this study; the full composition is given in Table 1. In each case, the core/shell weight ratio was 80/20 and the shell comonomer mixture contained 0.4 wt % DAAM. The cross-link density in this study was controlled only by the amount of ADH added (various levels below and up to the stoichiometric amount). The two latexes will be referred to as C80d0.1S20D0.4 and C80d0.15S20D0.4, respectively.

Experimental Techniques. *Tack Experiments.* Probe tack experiments were performed on our custom-designed probe tester, allowing simultaneous observation of the debonding process through the transparent glass substrate (16). During a probe tack test, a flat-ended probe of 1 cm diameter comes into contact with the adhesive film at 30 μm·s^{-1}. The probe stays in contact with the PSA layer for 1 s. The contact force is 70 N (corresponding to an average pressure of 1 MPa for a probe fully in contact). The probe is then removed at a debonding velocity between 10 and 1000 μm·s^{-1}. During the test, the force is recorded as a function of the probe displacement. Stress versus strain curves are then obtained by normalizing the force by the initial contact area between the probe and the adhesive layer and the displacement by the initial thickness of the PSA film.

The choice of stainless steel as a standard probe surface was dictated by convenience. To test different surfaces, a probe coated with polyethylene (PE) also was used. The degree of surface roughness, which can be important for soft adhesives (17−20), was well controlled in the case of stainless steel surfaces. The flat ends of the probes were first polished with several grades of abrasive paper until a final average root-mean-square (rms) roughness of 0.1 μm was found, as measured with an optical profilometer. The same probe was used throughout a series of tests, and its flat end was cleaned with water and acetone in the case of stainless steel and ethyl acetate in the case of PE.

Small-Strain Viscoelastic Properties. The performance of PSAs is related to their linear viscoelastic properties (21−24). In our case, because we were concerned with the effect of drying kinetics on the final properties of the film, the dynamic mechanical properties were investigated using a newly designed microrheometer (25, 26). The system is based on a sphere-on-flat contact configuration. During the test, the contact between a sapphire lens and the adhesive layer is made by applying a normal displacement to the lens. A normal force in the range of 0−2 N results from this contact. The lens, actuated by a piezoelectric actuator, is allowed to rotate about an axis parallel to the specimen surface. Its displacement is measured using a

noncontact displacement transducer (optical fiber). The tangential load is continuously monitored using a piezoelectric load cell with extended dynamics (from 10^{-2} to 10^3 Hz).

Rheological tests were performed at a small displacement amplitude (imposed shear strain $\gamma < 0.08$) using a sinusoidal displacement signal at a frequency between 0.1 and 10 Hz. These tests are aimed at providing an estimate of the commonly used rheological properties [storage modulus G', dissipative modulus G'', and the loss tangent $\tan(\delta)$] of the adhesive layer from the measurement of the dynamic contact stiffness. All linear rheological measurements have been performed at room temperature.

Tensile Experiments. Tensile tests were performed on a standard tensile testing machine (JFC TC3) equipped with a Hounsfield noncontacting laser extensometer, allowing accurate measurement of the strain even when the sample slips slightly between the clamps. The crosshead velocity was set equal to 50 mm $\cdot$ min^{-1}, corresponding to an initial strain rate of about 0.049 s^{-1}. All tests were carried out at room temperature. The force and displacement data were directly recorded from the tensile machine. Nominal stress (σ_N) and strain (λ) were then calculated using the initial value of the width, the thickness, and the initial distance between clamps.

3. RESULTS

The key process investigated in our study is the interparticle cross-linking taking place during the drying stage. Adhesive and linear rheological properties have been studied on C80d0.15S20D0.4, while adhesive properties and nonlinear elongational properties have been studied on C80d0.1S20D0.4. The only difference between these two materials is the amount of CTA added to the core, which varies from 0.1 % to 0.15 % DDM. This difference changes slightly the average molecular weight and gel fraction of the core so that the two materials are not absolutely comparable, but for the purpose of investigating the effects of cross-linking, the difference is not significant.

In each case, increasing amounts of ADH were added to the latexes. For both of these materials, the shells of the particles are very thin (typically 9 nm compared to the whole diameter of the particle of about 250 nm) and similar in chemical composition to the core. Thus, it is likely that there will be some mixing of shell copolymer with the underlying core copolymer (5). Nevertheless, in view of the synthesis method, there will be an overall structuring of the particles with DAAM groups concentrated near the surface of the particles, evidence for which has been obtained by atomic force microscopy (14). Hence, it is reasonable to assume that the cross-linking reaction occurs at or near the interface between particles during film formation and creates some chemical connections between two neighboring particles. At the levels of CTA used in the synthesis of the core copolymer, the adhesive films formed without added ADH have no measurable gel content (14). However, the samples with added ADH have gel contents that can increase to 59 % for 100 % ADH (14).

Tack Results. Tack experiments have been performed on C80d0.1S20D0.4 and C80d0.15S20D0.4 latexes to which various amounts of ADH were added to the latex prior to film formation. Probe tests were carried out on stainless steel probes and on PE-coated probes at debonding velocities of

10, 100, and 1000 μm $\cdot$ s^{-1}. Only the results for C80d0.1S20D0.4 at 100 μm $\cdot$ s^{-1} are shown in Figure 1 because the overall shape of the curves was the same for C80d0.15S20D0.4 and when using the other two speeds. Regardless of the cross-link density, a well-defined stress plateau was observed at intermediate strains, which is the signature of the fibrillating structure created from elongation of the microfoam resulting from cavitation in the adhesive film (27).

The peak stress was unchanged as the cross-link density increased, but the shape of the stress–strain curves changes markedly as a function of the ADH content. An adhesive film formed with no added ADH was characterized by a double fibrillation plateau at intermediate strains. The decrease in the stress of about 0.1 MPa is due to the air penetration in the middle of the adhesive layer (16, 28). The force then plateaus at a nonzero, constant value until the end of the test, leading to cohesive debonding where some residues of adhesive are left on the probe at the end of the test. For an adhesive film formed in the presence of added ADH (with cross-linking), air penetration no longer occurs. The walls of the cavities tend to extend vertically until the final detachment of the walls of the foam structure from the probe. An increasing degree of interparticle cross-linking leads to an earlier detachment of the fibrils and to a slight increase in the stress necessary to deform the fibrils. A comparison between the adhesive properties on PE and steel indicates that the debonding mechanism is not very sensitive to the low surface energy substrate, with the only difference being the detachment criterion of the fibrils, which occurs sooner for the PE substrate. This provides an indication that the interfacial cross-linking between particles must not have a large effect on the linear viscoelastic properties of the adhesive (10).

Standard Adhesive Test Results. Although these results are the focus of a separate publication (14), it is also interesting to discuss briefly how PSAs based on interfacially cross-linked particles behave in more standard adhesive tests such as peel adhesion and shear resistance. Cross-linking is known as a tool to improve the shear resistance of PSAs, but the effect on the peel adhesion is generally detrimental even at low cross-link densities (29). The activation of interfacial cross-linking during drying of soft and viscoelastic particles can, however, be an exception. As can be seen in Figure 2, a significant increase in the shear resistance is observed and is accompanied by only a slight decrease in the peel adhesion (only results on PE are shown here, but the trend is the same on stainless steel (14)). This suggests that the cross-linking process, which causes the fibrils to be less deformable in the probe tests, plays a fundamental role in controlling the shear resistance and that peel adhesion is more governed by intermediate-strain dissipation of the core, which is the major phase by volume.

If the PSA is comprised of homogeneous particles with cross-linking controlled only by the CTA, the same balance of the adhesive performance is not generally possible and any increase in the shear resistance typically leads to a decrease in the peel force. This different behavior led us to
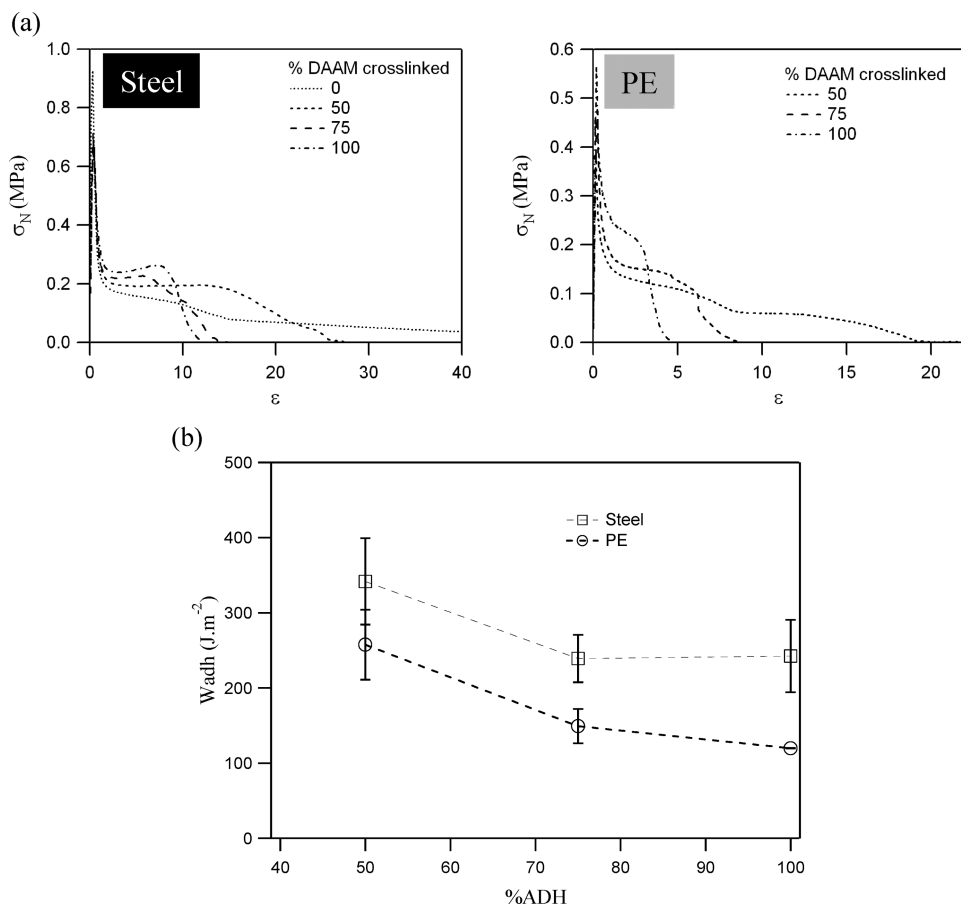
FIGURE 1. (a) Stress versus strain tack curves of C80d0.1S20D0.4 where 0, 50, 75, and 100% of the stoichiometric level of ADH was added. Tests were performed on stainless steel at 100 μm·s^{-1} (left) and on PE at 10 μm·s^{-1} (right). (b) Adhesion energies obtained at 100 μm·s^{-1} on stainless steel and on PE as a function of added ADH.
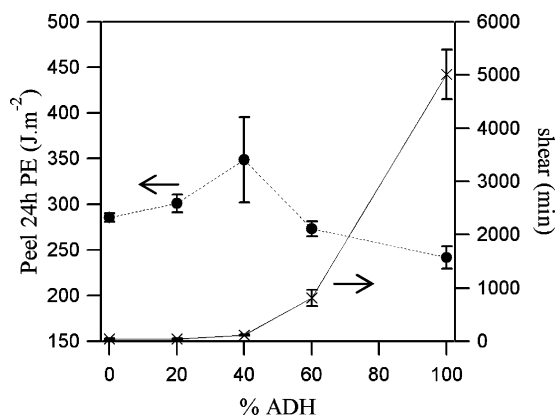

FIGURE 2. Shear resistance and peel performance of C80d0.1S20D0.4 as a function of the amount of ADH added.

investigate in more detail the viscoelastic properties of the materials in anticipation that this would help to explain the unusual adhesive behavior of these interfacially cross-linked core−shell PSAs.

Linear Viscoelastic Properties. The linear viscoelastic properties were measured on adhesive films made from C80d0.15S20D0.4 with 0, 23, 59, and 100% of the stoichiometric amount of ADH added to the latex prior to film formation.

From Figure 3, it is clear that the cross-link density has only a small effect on G' and G''. What also is important to

notice is that, in all cases, the shear modulus lies well below 0.1 MPa. Thus, the so-called Dahlquist criterion, which stipulates that the shear elastic modulus at the bonding frequency must be lower than 0.1 MPa for the layer to be able to form a good contact within the contact time, is always fulfilled. The constant value of G' also explains why no differences were observed on the peak stress values σ_{max} of the tack curves.

Figure 4 shows that there is an initial effect of activating the cross-linking reaction in reducing tan(δ), but further increases in the cross-link density then have a no effect on tan(δ) at high frequencies and cause only a slight decrease in tan(δ) at lower frequencies. This can be explained by the fact that short-range configurational changes that occur at high frequencies should be insensitive to the presence of cross-links while long-range motions at low frequencies are affected (30).

Despite their decrease with the cross-link density, tan(δ) values always stay above 0.5, which is a signature of a quite dissipative material regardless of the degree of cross-linking. The combination of highly dissipative properties in the linear regime with a low modulus gives a high value of tan(δ)/$G'(\omega)$ and is an ideal condition for the evolution of individual expanded cavities into an elongated microfoam structure on a low-adhesion substrate such as PE (26). This is the starting
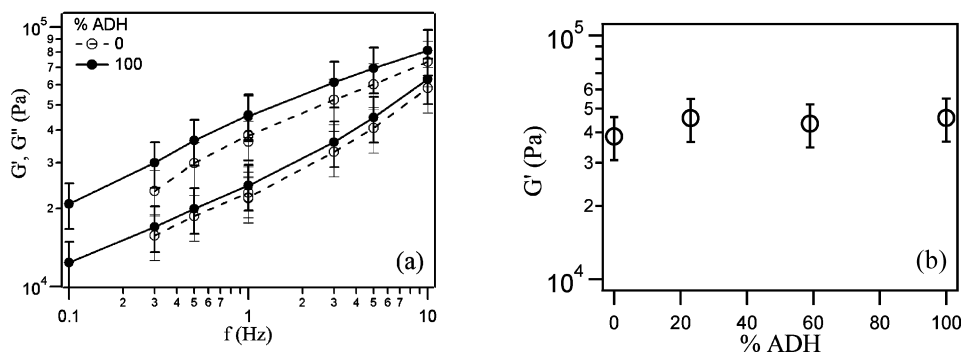
FIGURE 3. Linear rheological results of C80d0.15S20D0.4: (a) evolution of the storage (G') and loss (G'') moduli as a function of the frequency (○, un-cross-linked DAAM groups; ●, 100% of the stoichiometric amount of ADH added); (b) evolution of the shear elastic modulus as a function of the percentage of ADH added to the latex at $f = 1$ Hz.
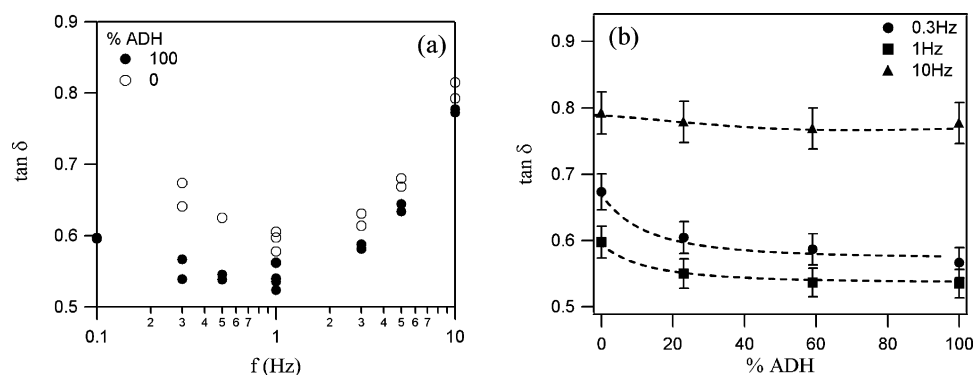

FIGURE 4. Linear viscoelastic properties of C80d0.15S20D0.4: (a) evolution of tan(δ) as a function of the frequency (○, un-cross-linked DAAM groups; ●, 100% of the stoichiometric amount of ADH added); (b) evolution of tan(δ) as a function of the fraction of ADH added to the latex at $f = 0.3$, 1, and 10 Hz.
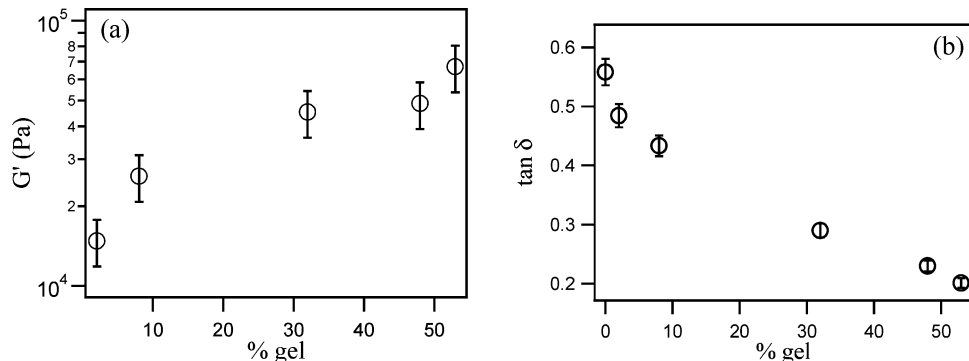

FIGURE 5. Linear rheological results of PnBA latexes differing by their gel contents: (a) evolution of the storage modulus G' as a function of the gel content at $f = 0.3$ Hz; (b) evolution of tan(δ) as a function of the gel content ($f = 0.3$ Hz) (after ref 9).

point of the fibrillating structure formation, which is one of the conditions required for high adhesive energy (31).

These results are in direct contrast to the situation where the degree of cross-linking is changed by varying the amount of cross-linking within each particle rather than between particles (2, 6, 9). An increase in I was observed, leading to a significant decrease in dissipation measured by I (Figure 5). Increasing the gel content in similar proportions but within the particles has been found to be detrimental to adhesion, especially on low-energy surfaces.

Large-Strain Properties. The large-strain properties of a soft material are a very sensitive probe of the network architecture of a polymer. Yet, the raw data curves are always highly nonlinear and are often used simply to obtain

a fracture strain or stress (32, 33). These characteristics are of very limited value for PSAs, which are expected to detach from a surface rather than break. On the other hand, the detailed shape of the stress−strain curve can be compared to molecular models of rubber elasticity and can reveal details about the network structure and molecular relaxation processes that will take place, for example, during a peeling process. We have recently proposed some analysis tools of the large-strain uniaxial tension curves, which are adapted to the characteristics of the soft sparsely cross-linked networks used in PSA applications (13, 26, 34). They are based on the analysis of the reduced stress σ_R, also called Mooney stress, obtained by normalizing the nominal stress by $\lambda - (1/\lambda^2)$, where λ is the extension ratio. This normalization
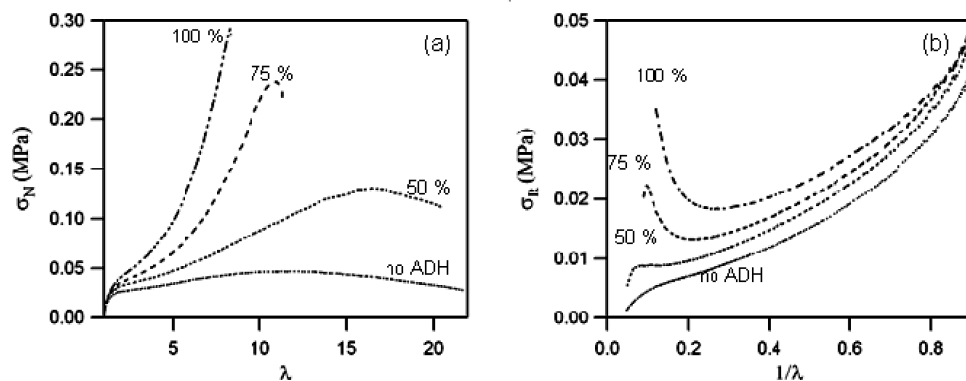
FIGURE 6. Tensile results of films formed with C80d0.1S20D0.4 where 0, 50, 75, and 100 % of the stoichiometric amount of ADH has been added: (a) nominal stress versus strain curves; (b) same results represented as Mooney stress σ_R as a function of $1/\lambda$.
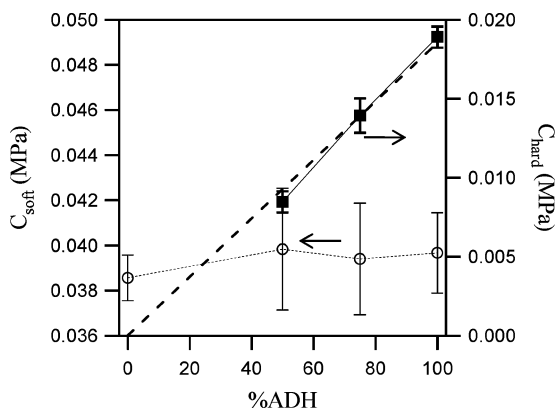

FIGURE 7. C_{soft} (empty circles) and C_{hard} (filled squares) of C80d0.1S20D0.4 as a function of the percentage of the stoichiometric amount of ADH added [the dashed line corresponds to a linear fit of $C_{hard} = f(\%$ ADH)].

gives a modulus as a function of λ, which reveals very clearly softening or hardening processes relative to a rubber obeying the simple theory of rubber elasticity.

Nominal stress versus strain tensile curves and their corresponding Mooney representations are shown in Figure 6. The effect of activation of the cross-linking and of further increases in the cross-link density on the tensile properties is considerable. In the absence of cross-linking, the tensile curve shows a pronounced softening above $\lambda = 2$ and the Mooney plot shows the absence of any hardening at small values of $1/\lambda$ (Figure 6b). Activation of the cross-linking does not alter the initial part of the curve but has a significant effect on the large-strain portion, and a marked strain hardening at large strain appears at a progressively lower strain.

Nonlinear Elastic Parameters. Two parameters can be compared quantitatively in the large-strain data: the extent of softening at intermediate strain and the minimum value of reduced stress.

Following the methodology previously proposed (26), which is described in the Supporting Information, we extracted from the tensile data the two parameters C_{hard} and C_{soft}, which are representative of the permanent and temporary cross-link points, respectively. The data are presented in Figure 7, and for all materials, C_{soft} is much larger than C_{hard}, which means that the modulus at small strains is governed more by temporary entanglements than by chemi-

cal cross-links. However, while C_{soft} appears to be approximately independent of the ADH content, C_{hard} increases markedly with ADH. This demonstrates clearly the effect of adding ADH on the creation of nonrelaxing permanent cross-links.

While the Mooney stress is very useful to have a quick assessment of the nonlinear properties of the PSA at a given tensile velocity, one has to keep in mind that acrylic PSAs, in particular, are markedly strain-rate-dependent. This rate dependence is supported by the fact that the maximal deformation of the fibrils is influenced significantly by the debonding velocity during tack experiments, as observed in Figure 8, in which the results for C80d15S20D0.4 with 100 % ADH added and for C80d1S20D0.4 with 75 % ADH added are shown.

Viscoelastic-Hardening Description. In order to account fully for the viscoelastic nature of the material without sacrificing the large-strain description, we can use a nonlinear viscoelastic model combining the properties of a viscoelastic fluid (representing the core) and a strain-hardening elastic solid (for the cross-linked shell). The simplest example of such a model (13), described briefly here, is the parallel combination of the upper convected Maxwell (UCM) model, classically used in fluid mechanics to describe the flow of viscoelastic fluids (35), with the Gent strain-hardening model (36), recently proposed to describe the fully elastic deformation of rubbery networks and including the finite extensibility of polymer chains in the network. A prediction of the uniaxial stress−strain curve can be extracted from the constitutive model and comes out as the sum of contributions to the stress from the UCM and Gent elements, which can be written as

$$\sigma_N(\lambda) = \sigma_{N,v}(\lambda) + \sigma_{N,e}(\lambda) \tag{1}$$

where

$$\sigma_{N,v}(\lambda) = \left(\frac{2G_v De}{1 - 2De}\left(1 - \exp\left(\frac{1 - 2De}{De}(\lambda - 1)\right)\right) + \frac{G_v De}{1 + De}\left(1 - \exp\left(-\frac{1 + De}{De}(\lambda - 1)\right)\right)\right)\lambda^{-1} \tag{2}$$
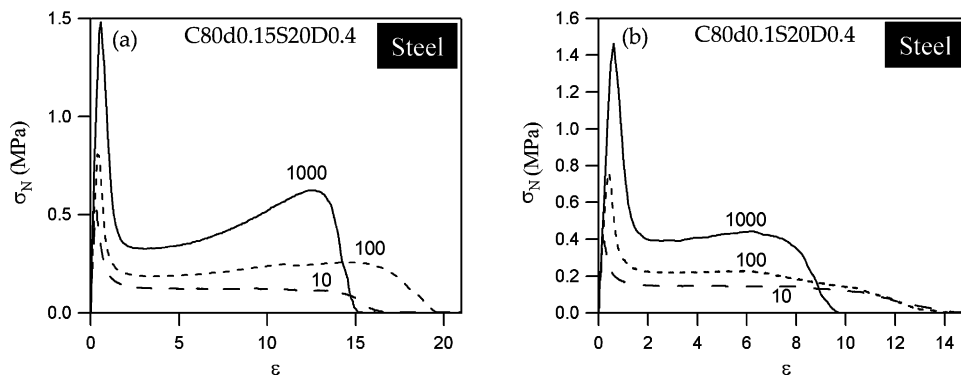
FIGURE 8. Stress versus strain tack curves (a) of C80d15S20D0.4 with 100% of the stoichiometric amount of ADH added and (b) of C80d1S20D0.4 with 75% of the stoichiometric amount of ADH added. Tests were performed on stainless steel at 10, 100, and 1000 $\mu m \cdot s^{-1}$.
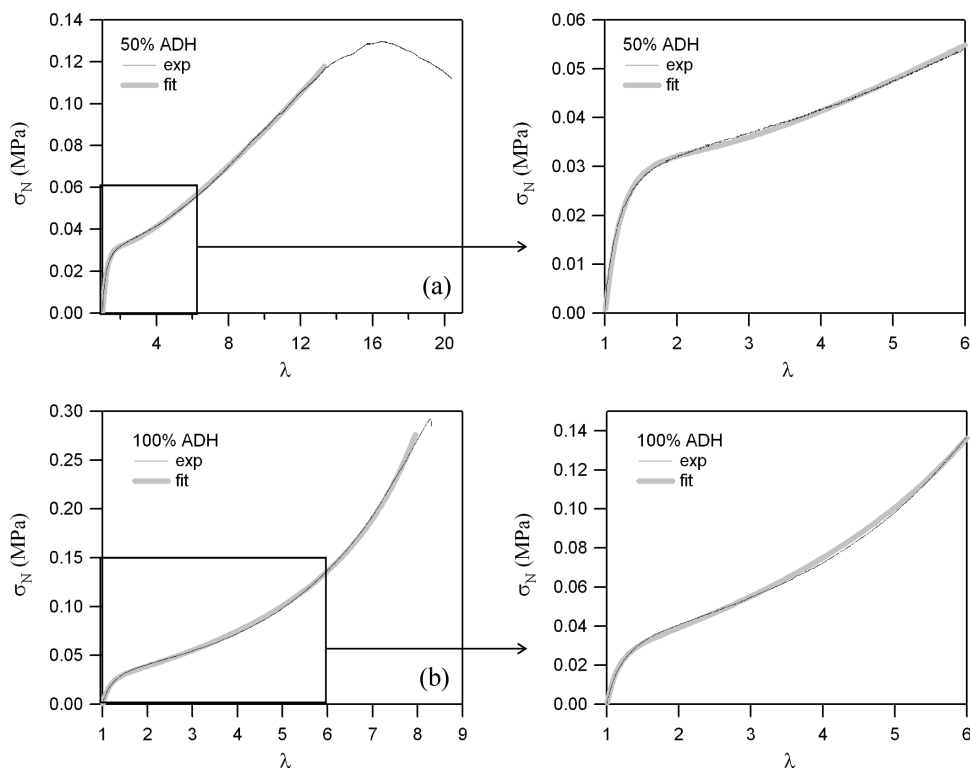

FIGURE 9. Two examples of C80d0.1S20D0.4 tensile curves fitted with the viscoelastic-hardening model: (a) 50% of the stoichiometric amount of ADH added; (b) 100% of the stoichiometric amount of ADH added. Magnifications of the curves in the intermediate range of deformations are given on the right.

and

$$\sigma_{N,e}(\lambda) = \left(\frac{G_e}{1 - \dfrac{\lambda^2 + 2/\lambda - 3}{J_m}} (\lambda^2 - 1/\lambda) \right) \lambda^{-1} \quad (3)$$

where G_v is the initial shear modulus of the viscoelastic part, De is the Deborah number (the product of the relaxation time of the viscous component and the strain rate), G_e is the small-strain shear modulus of the elastic part, J_m is the maximum allowable value of the first strain invariant, and λ is the extension ratio.

Two fitted tensile curves for C80d0.1S20D0.4 with 50% and 100% of the stoichiometric amount of ADH added are shown in Figure 9. With only 50% ADH, the tensile speci-men tends to flow and neck a little before breaking, which is why the ultimate strain part of the curve has not been fitted. From magnification of the curve given on the right, the intermediate strain behavior, which is of importance in controlling adhesion, seems to be correctly described by the model.

Table 2 shows the relevant parameters obtained from the fits of the tensile curves of C80d0.1S20D0.4. Each experimental tensile curve, among a series of three to five, was fitted separately, and Table 2 shows average values and standard deviations of the fit parameters.

An interesting result is that the values of G_e are low compared with those of G_v even at the highest cross-link density. This means that the network is only slightly cross-linked and does not participate much in the increase in the linear elastic modulus.

Table 2. Fitting Parameters Obtained in the Case of C80d0.1S20D0.4 without ADH and with 50, 75, and 100% of the Stoichiometric Amount of ADH Added

C80d0.1S20D0.4	G_v (kPa)	G_e (kPa)	J_m	De	G_v/G_e	$3(G_e + G_v)$ (kPa)
no ADH	30.6 (±2.11)	4.20 (±0.398)	10^6 imposed[a]	0.382 (±0.052)	7.30 (±0.284)	104 (±7.47)
50% ADH	47.4 (±9.73)	7.76 (±0.946)	3170 (±748)	0.211 (±0.068)	6.07 (±0.581)	165 (±31.9)
75% ADH	59.6 (±6.96)	11.9 (±1.01)	211 (±21.5)	0.126 (±0.030)	5.02 (±0.322)	215 (±23.5)
100% ADH	58.8 (±4.01)	16.0 (±0.507)	111 (±4.60)	0.114 (±0.021)	3.68 (±0.204)	224 (±13.0)

[a] For un-cross-linked liquidlike materials, the model cannot describe fully the behavior unless J_m is set to infinity ($J_m = 10^6$ has been chosen for the fits).
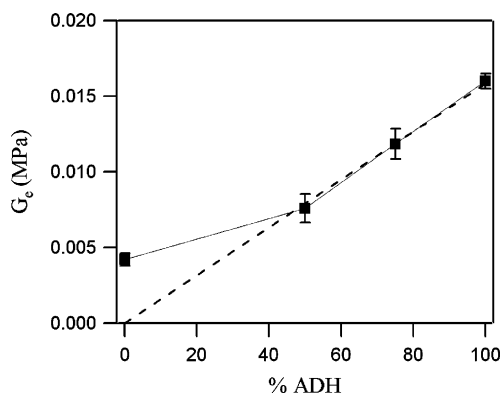

FIGURE 10. G_e of C80d0.1S20D0.4 as a function of the percentage of the stoichiometric amount of ADH added (the dashed line corresponds to a linear fit of $G_e = f(\%\ ADH)$).

A value as high as $J_m = 3000$, obtained when 50% ADH has been added, indicates that the cross-linked network is very extensible. This means that, for this polymer composition and with this amount of DAAM, an amount of ADH larger than 50% is required for the creation of a percolating network. Then, the decrease in J_m from 75% to 100% ADH could be related to the decrease in M_c as the cross-link density increases.

Also of interest is that, while both G_v and G_e increase with increasing cross-linking, G_e increases linearly with the amount of added cross-linker, whereas G_v has a weaker dependence on the level of added ADH.

Comments on Elastic vs Viscoelastic-Hardening Descriptions. Two different tools have been used for the study of the nonlinear properties: a nonlinear elastic representation and a nonlinear viscoelastic modeling. Results obtained with the two different methods are consistent with each other.

A few additional remarks can be made:

(i) Results from elastic and viscoelastic approaches show that, for this polymer composition (% DAAM), the percentage of the stoichiometric amount of ADH needed for the creation of a connected network is higher than 50%.

(ii) A comparison between Figures 7 and 10 emphasizes the possible analogy between C_{hard} and G_e. Both values tend to increase linearly as long as the material is cross-linked enough. C_{hard} is not defined for un-cross-linked materials, and the observed high value of G_e for 0% ADH may be attributed to a poor quality of the fits in this case.

4. DISCUSSION

We have analyzed in detail the rheological properties of two model waterborne PSAs in which interfacial cross-linking between particles was activated during film formation. The conventionally measured viscoelastic properties have shown very few changes due to the cross-linking process within the range of frequencies relevant for a tack or peel test. Yet, the nonlinear rheological properties characterized in uniaxial tension have proven to be very sensitive to changes in the interfacial cross-linking. It is interesting to discuss the effect that these changes have on the adhesive properties shown in Figures 1 and 2.

In the probe tests, increasing the interfacial cross-link density leads both to an increase in the fibrillation plateau stress and to a decrease in its extension both on stainless steel and on PE. The increase in stress with increasing cross-link density is observed clearly in the tensile curves. What is more interesting to notice is that, for higher levels of cross-linking, an increase in the cross-link density leads to a decrease in the maximal extension of the fibrils before debonding. This effect is much more pronounced on the low adhesion surface of PE than on the stainless steel surface (Figure 1).

There are two possible views for the description of the debonding of a fibrillar structure of an adhesive layer. In order to separate cleanly from the surface, the interface between the foot of the fibril and the surface must break. Previous authors have proposed that debonding of the fibrils should occur, either when a critical stress is reached (37, 38) or alternatively when enough elastic energy is released upon detachment to overcome the adhesive energy of the feet of the fibrils (39−42). Systematic and careful experiments with model materials will undoubtedly be needed to elucidate this point. In our system, increasing the cross-link density of the material leads most probably to an increase in the amount of stored elastic energy at large strains. We have seen that energy dissipation at intermediate strains is nearly constant as a function of the cross-link density (from values of C_{soft}) so the increase in the stored elastic energy could be due mainly to the increase in the stiffness of the percolating cross-linked phase.

From a more practical point of view (Figure 2), to reach an acceptable shear resistance, an increase in the cohesion at ultimate strains obviously is needed. At low levels of ADH, G_e seems sensitive to the presence of additional cross-links while J_m remains very high and this means that additional cross-links have been created (adding elastic strands to the small strain modulus) but probably the resulting networks are not fully percolating, resulting in very low shear resistance.

The dramatic increase in shear resistance observed between 60% and 100% ADH reflects the formation of a percolating network. Note that this percolating threshold is visible in J_m and in the maximum extension of the plateau between 50% and 75% ADH. On the other hand, increasing the cross-link density leads to a continuous increase in G_e. On the basis of these results, an optimal amount of ADH should be right at the percolation threshold to take advantage of the increase in the cohesion, leading to an improvement of the shear resistance without damaging peel adhesion, which is highly sensitive to the deformability of the polymer chains between cross-links.

5. CONCLUSION

In essence, we have shown that an interfacial cross-linking during the drying of the latex provides a means to have a very light but controlled level of cross-linking, which is entirely connected through the material. As we have shown, this tool, which is classically used for much harder coatings (43), requires fine-tuning when it is used for PSAs.

This low level of cross-linking does not modify significantly the small-strain modulus but significantly enhances the large-strain strength and allows the particle to keep a very soft and viscoelastic core. Using the conventional methods to control cross-linking inside each particle, the same balance is very difficult to achieve because any change in the level of CTA leads to a modification of the cross-linking structure, which affects both small- and large-strain properties and does not influence the softening.

Supporting Information Available: Schematic of the cross-linking chemical reaction and the procedure to measure and define the two constants C_{soft} and C_{hard} from tensile tests. This material is available free of charge via the Internet at http://pubs.acs.org.

REFERENCES AND NOTES

(1) Lindner, A.; Lestriez, B.; Mariot, S.; Brummer, R.; Maevis, T.; Lühmann, B.; Creton, C. *J. Adhesion* **2006**, *82*, 267–310.
(2) Tobing, S.; Klein, A.; Sperlinh, L.-H.; Petrasko, B. *J. Appl. Polym. Sci.* **2001**, *81*, 2109–2117.
(3) Gower, M. D.; Shanks, R. A. *Macromol. Chem. Phys.* **2004**, *205*, 2139–2150.
(4) Gower, M. D.; Shanks, R. A. *Macromol. Chem. Phys.* **2005**, *206*, 1015–1027.
(5) Stubbs, J. M.; Sundberg, D. C. *Prog. Org. Coat.* **2008**, *61*, 156–165.
(6) Zosel, A.; Ley, G. *Macromolecules* **1993**, *26*, 2222–2227.
(7) Aradian, A.; Raphael, E.; de Gennes, P. G. *Macromolecules* **2002**, *35*, 4036–4043.
(8) Tobing, S. D.; Klein, A. *J. Appl. Polym. Sci.* **2001**, *79*, 2558–2564.
(9) Josse, G.; PhD Thesis, Université Pierre et Marie Curie: Paris, 2001.
(10) Nase, J.; Lindner, A.; Creton, C. *Phys. Rev. Lett.* **2008**, *101*, 074503.
(11) Carelli, C.; Deplace, F.; Boissonnet, L.; Creton, C. *J. Adhes.* **2007**, *83*, 491–505.
(12) Wang, T.; Lei, C. H.; Dalton, A. B.; Creton, C.; Lin, Y.; Fernando, K. A. S.; Sun, Y.-P.; Manea, M.; Asua, J. M.; Keddie, J. L. *Adv. Mater.* **2006**, *18*, 2730–2734.
(13) Deplace, F.; Rabjohns, M. A.; Yamaguchi, T.; Foster, A. B.; Carelli, C.; Lei, C. H.; Ouzineb, K.; Keddie, J. L.; Lovell, P. A.; Creton, C. *Soft Matter* **2009**, *5*, 1440–1447.
(14) Foster, A. B. Lovell, P. A.; Rabjohns, M. A. *Polymer* **2009**, *50*, 1654–1670.
(15) Brandrup, J.; Immergut, E. H. *Polymer Handbook*; Wiley: New York, 1999.
(16) Lakrout, H.; Sergot, P.; Creton, C. *J. Adhes.* **1999**, *69*, 307–359.
(17) Fuller, K. N. G.; Roberts, A. D. *J. Phys. D: Appl. Phys.* **1981**, *14*, 221–239.
(18) Persson, B. N. J.; Albohr, O.; Creton, C.; Peveri, V. *J. Chem. Phys.* **2004**, *120*, 8779–8793.
(19) Chiche, A.; Pareige, P.; Creton, C. *C. R. Acad. Sci. Paris, Sér. IV* **2000**, *1*, 1197–1204.
(20) Chiche, A.; Dollhofer, J.; Creton, C. *Eur. Phys. J. E* **2005**, *17*, 389–401.
(21) Chang, E. P. *J. Adhes.* **1997**, *60*, 233–248.
(22) Tse, M. F.; Jacob, L. *J. Adhes.* **1996**, *56*, 79–95.
(23) Yarusso, D. J. *J. Adhes.* **1999**, *70*, 299–320.
(24) Tobing, S. D.; Klein, A. *J. Appl. Polym. Sci.* **2001**, *79*, 2230–2244.
(25) Gacoin, E.; Fretigny, C.; Chateauminois, A.; Perriot, A.; Barthel, E. *Tribol. Lett.* **2006**, *21*, 245–252.
(26) Deplace, F.; Carelli, C.; Mariot, S.; Retsos, H.; Chateauminois, A.; Ouzineb, K.; Creton, C. *J. Adhes.* **2009**, *85*, 18–54.
(27) Shull, K. R.; Creton, C. *J. Polym. Sci., Part B: Polym. Phys.* **2004**, *42*, 4023–4043.
(28) Poivet, S.; Nallet, F.; Gay, C.; Teisseire, J.; Fabre, P. *Eur. Phys. J. E* **2004**, *15*, 97–116.
(29) Satas, D. In *Handbook of pressure-sensitive-adhesives*, 2nd ed.; Satas, D., Ed.; Van Nostrand Reinhold: New York, 1989; Vol. 1, pp 396–456.
(30) Ferry, J. D. *Viscoelastic Properties of Polymers*, 3rd ed.; Wiley: 1980; Vol. 1.
(31) Léger, L.; Creton, C. *Philos. Trans. R. Soc. London, Ser. A: Math. Phys. Sci.* **2008**, *366*, 1425–1442.
(32) Zosel, A. *Colloid Polym. Sci.* **1985**, *263*, 541–553.
(33) Zosel, A. *Adv. Pressure Sensitive Adhes. Technol.* **1992**, *1*, 92–127.
(34) Roos, A.; Creton, C. *Macromolecules* **2005**, *38*, 7807–7818.
(35) Bird, R. B.; Armstrong, R. C.; Hassager, O. *Dynamics of Polymeric Liquids: Fluid Mechanics*, 2nd ed.; Wiley: New York, 1987; Vol. 1.
(36) Gent, A. N. *Rubber Chem. Technol.* **1996**, *69*, 59–61.
(37) Kaelble, D. H. *Trans. Soc. Rheol.* **1965**, *9*, 135–163.
(38) Glassmaker, N. J.; Hui, C. Y.; Yamaguchi, T.; Creton, C. *Eur. Phys. J. E* **2008**, *25*, 253–266.
(39) Drzal, P. L.; Shull, K. R. *J. Adhes.* **2005**, *81*, 397–415.
(40) Crosby, A. J.; Shull, K. R.; Lakrout, H.; Creton, C. *J. Appl. Phys.* **2000**, *88*, 2956–2966.
(41) Crosby, A. J.; Shull, K. R. *J. Polym. Sci., Part B: Polym. Phys.* **1999**, *37*, 3455–3472.
(42) Creton, C.; Lakrout, H. *J. Polym. Sci., Part B: Polym. Phys.* **2000**, *38*, 965–979.
(43) Taylor, J. W.; Winnik, M. A. *J. Coat. Technol. Res.* **2004**, *1*, 163–190.

AM9003792